ISSN: 1410-8917
Jurnal Kimia Sains & Aplikasi
e-ISSN: 2597-9914

Jurnal Kimia Sains dan Aplikasi 29 (3) (2026): 186-194

Jurnal Kimia Sains dan Aplikasi
Journal of Scientific and Applied Chemistry

Journal homepage: http://ejournal.undip.ac.id/index.php/ksa

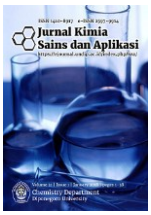

Cryogenic Microstructure Engineering of PVDF-Based Composite Membranes Doped with Alumina and Reduced Graphene Oxide Derived from Palm Kernel Shell (PKS)

Meilysa Yonara [1], Delovita Ginting [1,*], Romi Fadli Syahputra [1], Asanah Radhi [2]

[1] Department of Physics, Faculty of Mathematics and Natural Sciences, Universitas Muhammadiyah Riau, Pekanbaru, Indonesia
[2] Faculty of Bioengineering and Technology, Universiti Malaysia Kelantan, Kelantan, Malaysia

* Corresponding author: delovita@umri.ac.id

https://doi.org/10.14710/jksa.29.3.186-194

Article Info

Article history:

Received: 24th December 2025
Revised: 02nd March 2026
Accepted: 02nd March 2026
Online: 22nd April 2026

Keywords:
solid polymer electrolytes; cryogenic engineering; PVDF composite membrane; reduced graphene oxide (rGO); palm kernel shell (PKS)

Abstract

Composite polymer membranes based on polyvinylidene fluoride (PVDF) have attracted attention as potential solid-state electrolyte candidates due to their thermal stability and mechanical robustness. However, microstructural heterogeneity and transport limitations remain key challenges. This study investigates the effect of cryogenic treatment (Series A) and rGO incorporation (Series B) on PVDF/Al_2O_3/CA composite membranes derived from palm kernel shell (PKS)-based reduced graphene oxide (rGO). Morphological characterization showed a reduction in pore size from 13–15 µm in the untreated membrane to 1.7–2.6 µm in the 2-minute treatment, improving membrane uniformity. UV–Vis spectroscopy revealed an increase in apparent optical band gap from 1.34 eV to 1.44 eV with increasing cryogenic duration, suggesting improved structural ordering within the composite membrane. Cyclic voltammetry (CV) measurements conducted under aqueous Na_2SO_4 conditions showed increased current response and capacitance with increasing rGO content (Series B), indicating enhanced interfacial electrochemical behavior. Electrochemical impedance spectroscopy (EIS) performed on Series A samples demonstrated a decrease in area-specific bulk resistance from 0.14 to 0.10 Ω·cm², corresponding to an apparent ionic conductivity of 8.0×10^{-2} S/cm under the applied aqueous screening configuration. The results indicate that cryogenic treatment primarily governs bulk resistance reduction through pore refinement, while rGO incorporation enhances electrochemical response under model aqueous conditions. These findings highlight the role of structural control and biomass-derived carbon fillers in tailoring composite membrane electrochemical characteristics.

1. Introduction

Rechargeable lithium-based energy storage systems have become widely adopted in portable electronics and electric vehicles due to their high energy density and operational stability [1]. One recent innovation in lithium-ion battery development is the use of solid polymer electrolyte (SPE), which offers higher thermal stability, longer service life, and improved safety compared to conventional liquid electrolytes [2]. Despite these advantages, SPE still faces limitations such as low ionic conductivity at ambient temperature and sensitivity to moisture [3]. In solvent-free solid polymer electrolytes (salt-in-polymer systems), room-temperature ionic conductivity typically ranges from 10^{-5} to 10^{-3} S cm^{-1}, depending on the polymer matrix, salt concentration, and plasticization. Composite polymer electrolytes incorporating ceramic fillers may improve conductivity by one to two orders of magnitude, while gel- or hydrogel-based systems containing a significant liquid phase can reach 10^{-2} to 10^{-1} S cm^{-1}. Therefore, careful distinction between these systems is essential when interpreting conductivity values and electrochemical response parameters. In this context, electrochemical

measurements, such as apparent capacitance derived from cyclic voltammetry, are interpreted as indicators of interfacial polarization rather than intrinsic charge-storage properties of the electrolyte material itself [4].

To address these issues, various additives have been introduced. Reduced graphene oxide (rGO) possesses superior mechanical strength and electrical conductivity, and it can be produced sustainably from carbon-rich palm kernel shell (PKS) biomass [5]. In addition, alumina (Al_2O_3) is recognized as an effective reinforcing material that enhances the thermal stability and safety of SPE. The combined incorporation of rGO and Al_2O_3 may modify polymer crystallinity, interfacial interactions, and microstructural homogeneity. rGO is expected to facilitate conductive pathway formation and improve interfacial charge transfer, while Al_2O_3 can act as a ceramic stabilizing filler that disrupts excessive crystallinity and enhances polymer–filler interaction [6].

Further improvement can be achieved through the application of cryogenic engineering, which involves processing below -150°C. Rapid cryogenic quenching reduces molecular mobility, suppresses large-scale phase separation during solvent evaporation, increases nucleation density, and limits spherulitic growth within semicrystalline PVDF matrices. In PVDF/CA/filler systems, this may alter crystallization kinetics and promote a more homogeneous pore distribution [7]. Cryogenic treatment has been shown to improve microstructural uniformity and interfacial stability of polymer-based electrolyte systems [8]. However, studies that comprehensively integrate rGO from PKS, alumina, and cryogenic processing remain limited.

The present study focuses on the synthesis of PVDF-based composite membranes incorporating Al_2O_3 and biomass-derived rGO, engineered via controlled cryogenic treatment to investigate structural and electrochemical response behavior. The effects of cryogenic treatment on morphology, crystallization behavior, bulk resistance, and electrochemical impedance response were systematically evaluated. The use of rGO derived from palm kernel shell (PKS) additionally contributes to sustainable material utilization by valorizing agricultural biomass waste [9]. This work aims to elucidate the synergistic effects of cryogenic microstructure control and rGO–Al_2O_3 incorporation on the electrochemical behavior of composite membranes, providing insight for future electrolyte material development.

2. Experimental

2.1. Materials and Equipment

The materials used in this study include alumina nanoparticles (Al_2O_3), polyvinylidene fluoride (PVDF), cellulose acetate (CA), reduced graphene oxide (rGO), N,N-Dimethylacetamide (DMAc, 99.5%) as a solvent, and deionized water as an additive solvent and washing medium. Activated carbon derived from palm kernel shell (PKS) was used as a sustainable carbon precursor for the synthesis of graphene oxide (GO) prior to reduction to rGO.

Table 1. Composition of PVDF-based composite membranes (wt% of total solid content) A: cryo-time, 0% rGO | B: rGO% at 0 min cryo | C: cryo-time at 15% rGO

Sample name	PVDF (%)	Al_2O_3 (%)	CA (%)	rGO-PKS (%)	Cryogenic time (minute)
A1	70	25	5	0	0
A2	70	25	5	0	2
A3	70	25	5	0	4
B1	70	25	5	5	0
B2	70	25	5	10	0
B3	70	25	5	15	0
C1	70	25	5	15	0
C2	70	25	5	15	2
C3	70	25	5	15	4

All values are wt% relative to total solid content (PVDF + Al_2O_3 + CA + rGO = 100 wt%). Series definitions: A = cryogenic time variation with 0% rGO; B = rGO content variation without cryogenic treatment; C = cryogenic time variation at fixed 15% rGO.

The instrumentation included a magnetic stirrer, ultrasonicator, spin coater, oven, Teflon-coated autoclave, freeze dryer, scanning electron microscope (SEM), UV–Visible (UV–Vis) spectrophotometer, digital micrometer, and Solartron Electrochemical Interface 1286 for cyclic voltammetry (CV) and electrochemical impedance spectroscopy (EIS).

2.2. Synthesis of Reduced Graphene Oxide from Palm Kernel Shell

Graphene oxide (GO) was synthesized from activated carbon derived from palm kernel shell using a modified Hummers method. 1 gram of activated carbon was dispersed in 25 mL of concentrated sulfuric acid under continuous stirring in an ice bath. Three grams of potassium permanganate ($KMnO_4$) were gradually added to oxidize the carbon for three hours. Distilled water was slowly introduced, followed by hydrogen peroxide (H_2O_2) to reduce residual $KMnO_4$. The mixture was centrifuged, washed thoroughly, and dried at 90°C for 12 hours to obtain GO powder. Reduction of GO into rGO was performed via a hydrothermal method. Forty milligrams of GO were dispersed in 200 mL of distilled water and sonicated to achieve a homogeneous suspension. Reducing agents, including hydrazine hydrate, tin(II) chloride dihydrate ($SnCl_2{\cdot}2H_2O$), and ammonium hydroxide (NH_4OH), were added to induce hydroxide formation. The mixture was heated in a Teflon-coated autoclave at 120°C for six hours. The resulting rGO nanocomposite powder was washed, dried, and characterized using XRD to confirm the removal of oxygen-containing functional groups and improvement in graphitic quality [10].

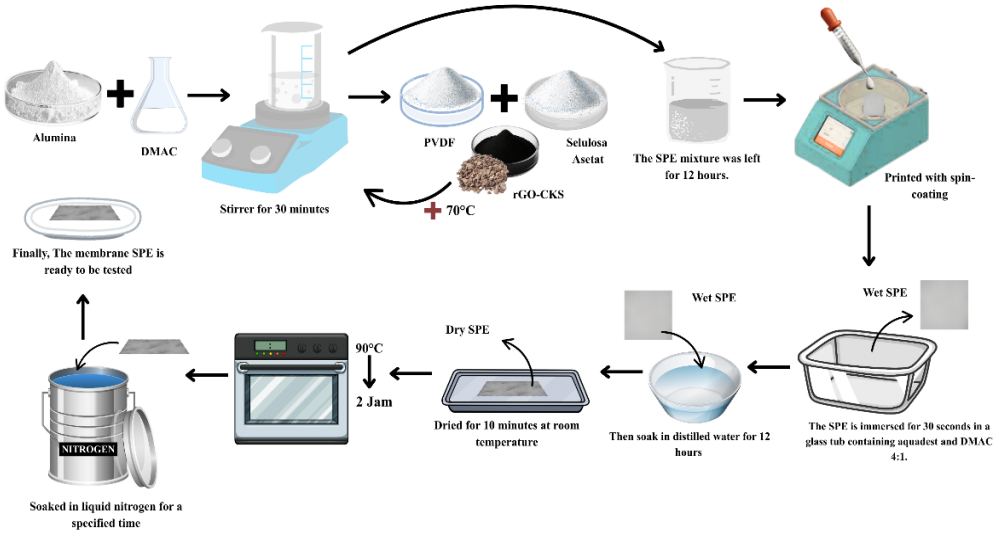

Figure 1. Schematic of the SPE fabrication process

2.3. Fabrication of SPE Membranes

Alumina nanoparticles (0.75 g) were dispersed in 21 mL of DMAc with stirring for 30 minutes, then heated to 70°C. Predetermined amounts of PVDF, CA, and rGO (varied compositions) were added and stirred until a homogeneous solution was obtained. The solution was ultrasonicated for 30 minutes and left for 12 hours. The homogeneous solution was deposited onto a clean glass substrate using spin coating at 3000 rpm for 60 seconds to obtain uniform thin films. The resulting thin film was detached by immersion in a coagulation bath containing DMAc: deionized water (1:4) for 30 seconds, followed by immersion in pure deionized water for 12 hours to remove residual solvents [11].

2.4. Cryogenic Treatment

Prior to cryogenic immersion, membranes were preheated at 90°C for two hours to remove residual solvent and promote initial polymer chain relaxation. This step ensures a controlled semicrystalline starting structure before rapid quenching. The membranes were then immersed in liquid nitrogen for 0, 2, or 4 minutes to evaluate the effect of cryogenic treatment duration. Rapid quenching in liquid nitrogen suppresses large-scale phase separation, increases nucleation density, and limits spherulitic growth in semicrystalline PVDF-based systems, thereby refining pore morphology [12]. Samples were stabilized at room temperature for one hour prior to characterization [13].

2.5. Characterization Techniques

2.5.1. The X-ray Diffraction (XRD) of GO and rGO

The X-ray diffraction (XRD) pattern of GO exhibits a main diffraction peak at $2\theta \approx 10°$ corresponding to the (001) plane, along with a weak peak around 26° assigned to the (002) plane. In contrast, rGO shows the disappearance of the (001) peak and the emergence of a dominant peak at $2\theta \approx 26°$ corresponding to the (002) plane.

This peak shift indicates the removal of oxygen-containing functional groups and a higher degree of reduction, confirming the restoration of the graphitic layered structure. The calculated interlayer spacing (d-spacing) of approximately 0.34 nm suggests a structure approaching that of graphite, accompanied by improved crystallinity [14].

The obtained diffraction pattern (Figure 2) confirms the successful reduction of GO to rGO via a combined chemical and thermal process. This structural transformation is consistent with the typical characteristics of conductive carbon materials and supports their suitability as conductive fillers in PVDF-based composite membranes.

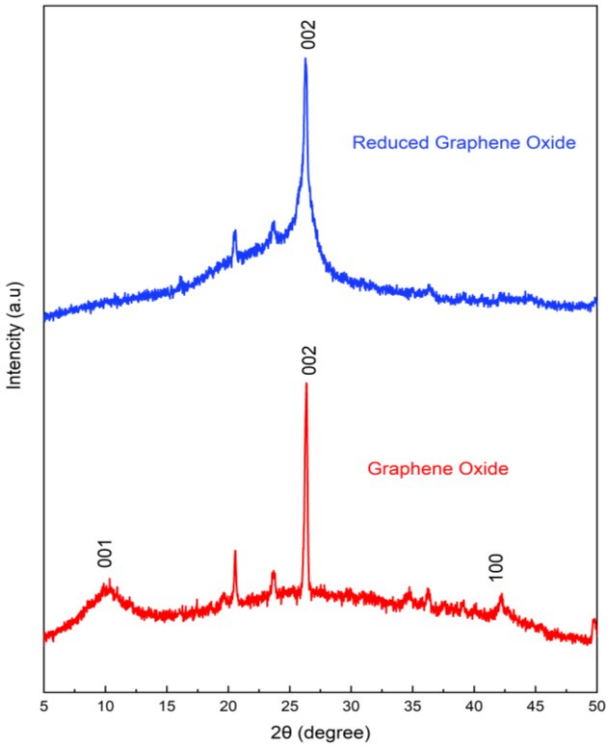

Figure 2. XRD patterns of GO and rGO

2.5.2. Membrane Thickness Measurement

Membrane thickness (L) was measured using a FRANK–PTI GmbH Universal Micrometer (Type S16502 0000, Germany) with ±1 µm accuracy, following general procedures consistent with ASTM D374 standard for thickness measurement of solid polymer films [15]. Prior to measurement, the membranes were conditioned at room temperature (25 ± 2°C) for 24 hours to ensure dimensional stability and eliminate residual solvent effects. Thickness was recorded at five different positions on each sample to account for spatial variation, and the average value was used for ionic conductivity calculations ($\sigma = L/(R_b \times A)$). The relative standard deviation of the measurements was maintained below 5%, indicating acceptable thickness uniformity among samples.

2.5.3. Scanning Electron Microscopy (SEM)

The surface morphology of the samples was examined using a JEOL JSM-IT100 scanning electron microscope (SEM). Prior to imaging, the samples were sputter-coated with a thin layer of gold/palladium to enhance surface conductivity. Micrographs were obtained at a magnification of 500×, and additional magnifications were used to observe finer structural features. Morphological analysis focused on pore size, uniformity, and distribution to assess the effects of cryogenic treatment and rGO–Al_2O_3 doping [16].

2.5.4. UV–Vis Spectroscopy

The optical properties of the samples were measured using a Shimadzu UV-2600 UV–Visible spectrophotometer equipped with an integrating sphere attachment for diffuse reflectance and transmittance measurements. Spectra were recorded over the wavelength range of 185–1100 nm, covering ultraviolet and visible-near infrared regions. Baseline correction was performed prior to each measurement using a reference standard to minimize instrumental artifacts. Peak shifts and absorption intensities were analyzed to confirm the reduction of graphene oxide to rGO and to investigate polymer chain regularity [17].

2.5.5. Cyclic Voltammetry (CV)

Cyclic voltammetry (CV) measurements were conducted to compare the electrochemical response of the composite membranes under aqueous model conditions. Measurements were conducted using a Solartron Electrochemical Interface 1286 connected to a conventional three-electrode system. A platinum wire was used as the counter electrode, a saturated Ag/AgCl (3 M KCl) electrode served as the reference, and the working electrode was prepared by coating SPE membrane pieces on a conductive substrate. The electrolyte solution (1 M Na_2SO_4) was purged with high-purity nitrogen gas for at least 15 minutes to remove dissolved oxygen. The potential range was scanned between −0.2 V and 0.8 V at various scan rates (5, 10, 20, 50, and 100 mV s^{-1}).

CV curves were analyzed to examine current response and interfacial behavior. Specific capacitance values were reported only as comparative electrochemical response indicators and not as intrinsic electrolyte performance parameters. It should be noted that the three-electrode aqueous configuration does not represent a lithium-ion cell environment but was employed as a screening platform to compare electrochemical response trends among samples. All measurements were repeated at least three times to ensure reproducibility [18].

2.5.6. Electrochemical Impedance Spectroscopy (EIS)

Electrochemical Impedance Spectroscopy (EIS) was conducted at the Electrochemistry Laboratory, Institut Teknologi Sepuluh Nopember (ITS), using a Solartron Electrochemical Interface 1286 Galvanostat to determine ionic resistance (bulk resistance) and evaluate ionic conductivity of SPE membranes subjected to cryogenic treatment and rGO–Al_2O_3 doping. EIS measurements were conducted in a three-electrode aqueous configuration (1 M Na_2SO_4) to evaluate impedance response under identical screening conditions.

Measurements were carried out over a frequency range of 1 Hz to 1 MHz with a voltage amplitude of 10 mV at room temperature. This configuration does not isolate intrinsic through-plane bulk resistance as in a symmetric blocking electrode setup (e.g., SS|membrane|SS). Therefore, the extracted bulk resistance reflects a composite electrochemical response under aqueous conditions rather than intrinsic Li^+ transport within a dry solid-polymer electrolyte. Nyquist plots were used to analyze impedance data, with bulk resistance (R_b) determined from the intersection of the curve with the real axis (Z′). Data processing was performed using Origin software to extract bulk resistance (R_b) and charge-transfer resistance (R_{ct}) values. Ionic conductivity (σ) was calculated using Equation (1).

$$\sigma = \frac{L}{R_b \times A} \quad (1)$$

Where, σ is the ionic conductivity of the membrane (S cm^{-1}), L is the membrane thickness (cm), R_b is the bulk resistance obtained from the high-frequency intercept of the Nyquist plot (Ω), and A is the effective contact area between the membrane and electrode (cm^2) [19].

3. Results and Discussion

3.1. Membrane Thickness

The thickness of SPE membranes was measured to evaluate the effect of cryogenic treatment on dimensional stability [20]. The measured thickness values ranged between 77 and 81 µm across all samples, with no significant variation as a function of cryogenic treatment duration. For example, samples A1, A2, and A3 exhibited average thickness values of 80 ± 1 µm, 80 ± 1 µm, and 81 ± 1 µm (mean ± standard deviation, n = 5), respectively. The small variation indicates that cryogenic treatment duration does not significantly affect membrane thickness. Thickness uniformity is more likely governed by casting consistency and dispersion homogeneity of PVDF, Al_2O_3, CA, and rGO within the precursor solution rather than by post-treatment cryogenic exposure. A summary of the SPE thickness measurement results is presented in Table 3.

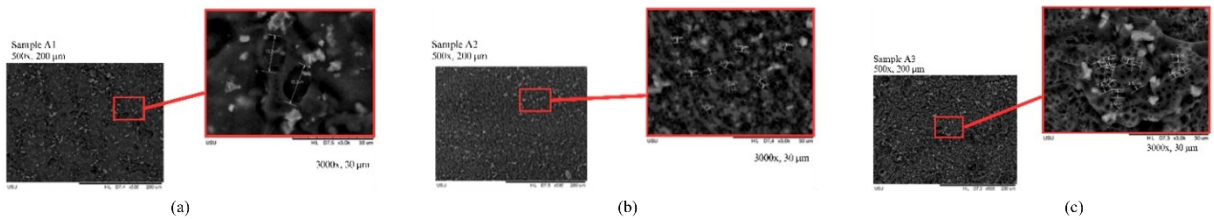

Figure 3. SPE surface morphology of Series A membranes at 500× (200 µm scale) and 3000× (30 µm scale): (a) A1, (b) A2, and (c) A3

Table 3. Results of SPE membrane thickness measurements

Sample	Membrane thickness (µm)
A1	80 ± 1
A2	80 ± 1
A3	81 ± 1
B1	80 ± 1
B2	80 ± 1
B3	80 ± 1
C1	80 ± 1
C2	81 ± 1
C3	80 ± 1

Values are expressed as mean ± standard deviation (n = 5).

3.2. Scanning Electron Microscopy (SEM)

Scanning electron microscopy (SEM) analysis revealed a strong influence of cryogenic treatment on pore structure [21], as shown in Figure 3. Untreated membranes (A1) exhibited relatively large and irregular pores in the range of approximately 13–15 µm. This non-uniform pore distribution can lead to uneven ion transport pathways. With increasing cryogenic duration (A2 and A3), pore size was significantly reduced to approximately 2–4 µm, accompanied by improved pore distribution uniformity [22]. In contrast, sample A2 treated cryogenically for 2 minutes shows a significant reduction in pore size to approximately 1.7–2.6 µm, accompanied by a more homogeneous distribution of fillers. The reduction in pore size indicates improved structural compactness and reduced void heterogeneity within the membrane matrix. Sample A3, treated for 4 minutes, still exhibits relatively small pores (2–3 µm); however, partial filler agglomeration begins to appear. This densification suggests that extended cryogenic exposure further suppresses pore growth and promotes microstructural refinement.

Overall, these results confirm that cryogenic treatment effectively controls pore growth, reduces average pore diameter by approximately 87%, and enhances morphological uniformity. The present SEM analysis focuses exclusively on Series A (0% rGO) to isolate the effect of cryogenic treatment. Morphological evaluation of rGO-containing samples was not conducted in this study, and therefore, no direct conclusions regarding filler–cryo synergistic effects can be drawn [23].

3.3. UV-Vis

UV–Vis diffuse reflectance spectroscopy was conducted using a Shimadzu UV-2600 spectrophotometer in the wavelength range of 200–1000 nm [24]. The apparent optical band gap values, estimated using the Kubelka–Munk function and Tauc relation (assuming an indirect allowed transition), increased from 1.34 eV for A1 to 1.40 eV for A2 and 1.44 eV for A3. This increase suggests improved structural ordering and reduced defect-related absorption within the composite membranes after cryogenic treatment. The observed blue shift and reduced absorbance intensity may be associated with denser polymer chain packing and refined microstructure in sample A3.

Therefore, the 4-minute cryogenic treatment (A3) is considered optimal in terms of structural refinement, which correlates with reduced bulk resistance observed in EIS measurements [25]. It should be noted that PVDF is a wide-band-gap polymer, and the calculated values represent apparent optical transitions of the composite system rather than the intrinsic semiconductor band structure. The extracted band gap values may be influenced by light scattering, π–π interactions in rGO, defect states, and film thickness. Therefore, the interpretation is limited to comparative structural analysis among samples.

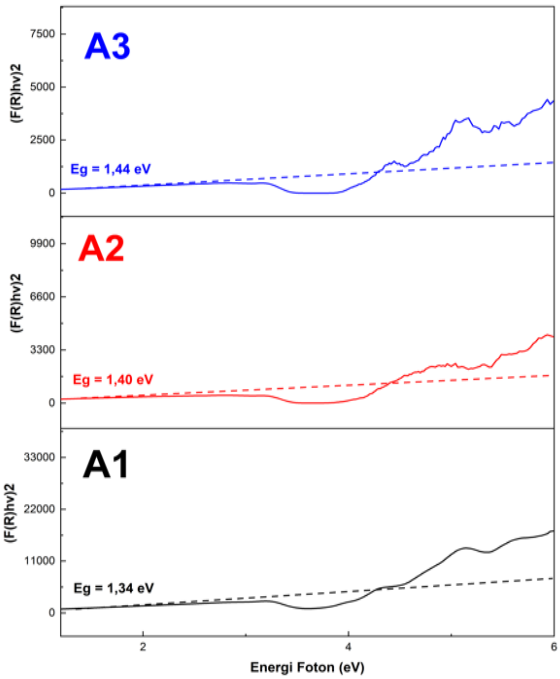

Figure 4. UV–Vis spectra of SPE membranes: (a) A1, (b) A2, and (c) A3

Table 4. UV–Vis characterization results of SPE membranes

Sample	Wavelength (nm)	λ_{max} (A)
A1	272	0.5910
A2	268	0.3367
A3	266	0.2940

3.4. Cyclic Voltammetry (CV)

Cyclic voltammetry (CV) measurements were performed using a Solartron Interface 1286 to comparatively evaluate the electrochemical response behavior of the composite membranes under aqueous Na_2SO_4 model conditions [26], as shown in Figure 5. At a scan rate of 0.02 V s^{-1}, sample A1 exhibited low peak currents (±0.005/−0.003 A) and a specific capacitance of 8.09 F g^{-1}, a relatively weak interfacial electrochemical response.

Sample A2 showed increased peak currents (±0.005/−0.004 A) and a higher specific capacitance of 13.82 F g^{-1}, enhanced electrochemical activity associated with cryogenic-induced structural refinement. The most significant enhancement was observed in sample A3, which exhibited peak currents of ±0.019/−0.009 A and the highest specific capacitance of 50.81 F g^{-1}. For comparison, a commercial cellulose-based filter paper (Whatman Grade 1) was tested as a porous reference under identical aqueous experimental conditions, yielding a specific capacitance of 29.63 F g^{-1}. This value was lower than that obtained for sample A3 under the same measurement configuration. These results suggest that cryogenic treatment improves the electrochemical response of the composite membrane, as reflected by increased CV curve area and current density (Table 5). It should be emphasized that the CV measurements were conducted in a three-electrode aqueous configuration and therefore represent comparative electrochemical screening rather than intrinsic lithium-ion electrolyte performance. The specific capacitance values reflect interfacial charge storage behavior within the composite membrane under the applied testing conditions.

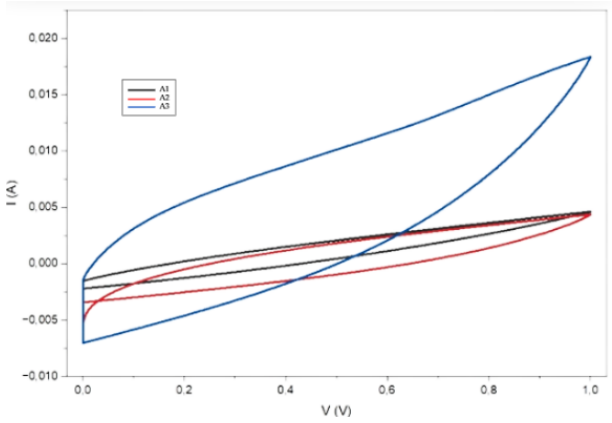

Figure 5. Cyclic voltammetry results of SPE membranes with varying cryogenic treatment durations

Table 5. Cyclic voltammetry characterization results of SPE membranes

Sample	Scan rate (V/s)	Specific Capacitance (F/g)	Positive Peak Current (A)	Negative Peak Current (A)
A1	0.02	8.087	0.005	-0.003
A2	0.02	13.8245	0.005	-0.004
A3	0.02	50.8115	0.019	-0.009
Whatman	0.02	29.6325	0.010	-0.005

The effect of rGO content on electrochemical performance is shown in Figure 6. Increasing rGO content results in a larger CV curve area and higher peak current, indicating enhanced interfacial electrochemical activity associated with the conductive nature of rGO [27]. Sample B1 exhibited the lowest peak current (0.0013 A) and specific capacitance of 104.98 F g^{-1}, while sample B3 showed the highest peak current (0.0025 A) and maximum specific capacitance of 139.77 F g^{-1}. This trend (B3 > B2 > B1) confirms that increasing rGO content enhances charge storage response and electrical interaction within the composite membrane under aqueous conditions. Since CV measurements were performed only for Series A and Series B, no direct conclusions regarding combined cryogenic–rGO synergistic effects can be established in the present study.

Table 6. Cyclic voltammetry characterization results with varying rGO content

Sample	Scan rate (V/s)	Specific capacitance (F/g)	Peak current (A, relative order)
B1	0.02	104,98	0.0013
B2	0.02	124,51	0.0017
B3	0.02	139,77	0.0025

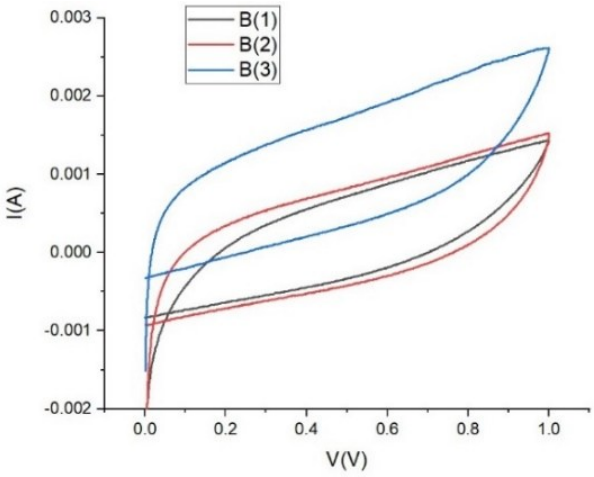

Figure 6. Cyclic voltammetry results of SPE membranes with varying rGO content

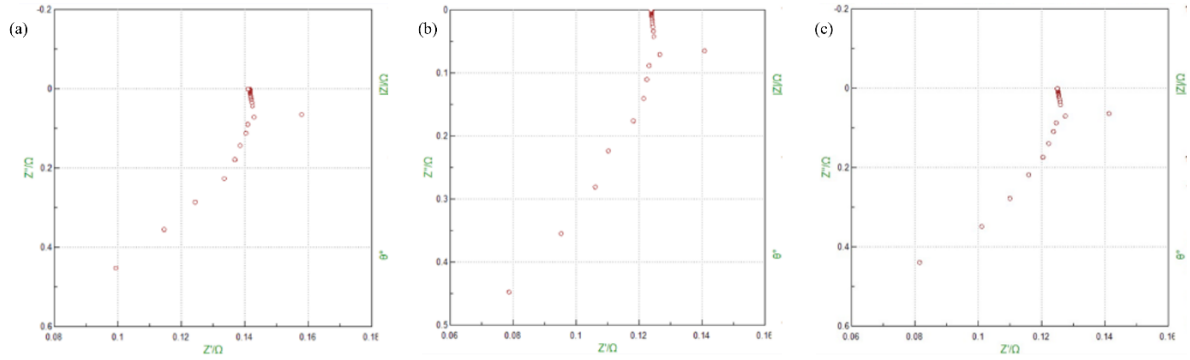

Figure 7. Nyquist plots of SPE membranes obtained from EIS measurements: (a) A1, (b) A2, and (c) A3

3.5. Electrochemical Impedance Spectroscopy (EIS)

Electrochemical impedance spectroscopy (EIS) results indicate that the apparent ionic conductivity increases with increasing cryogenic treatment duration. Nyquist plots (Figure 7) show a decrease in bulk resistance (R_b) from 0.14 Ω for A1 to 0.10 Ω for A3. Correspondingly, the calculated apparent conductivity increased from 5.7×10^{-2} S cm^{-1} (A1) to 8.0×10^{-2} S cm^{-1} (A3), based on Equation (1).

The reduction in R_b is attributed to improved microstructural homogeneity and reduced pore irregularity induced by cryogenic treatment, as observed in SEM analysis. Since EIS measurements were conducted only for Series A (0% rGO), the observed impedance reduction reflects the effect of cryogenic treatment alone [28]. Overall, the 4-minute cryogenic-treated membrane (A3) exhibits the lowest bulk resistance and highest apparent conductivity under the applied aqueous testing configuration.

It should be emphasized that the three-electrode aqueous configuration does not isolate intrinsic lithium-ion transport within a dry solid polymer electrolyte. Therefore, the reported conductivity values represent apparent ionic behavior under Na_2SO_4 model conditions rather than intrinsic Li^+ conductivity. The magnitude of the measured conductivity falls within the range typically observed for hydrated or aqueous-assisted systems and therefore should not be directly compared with dry PVDF-based solid polymer electrolytes reported for lithium battery applications.

Table 7. EIS characterization results of SPE membranes

Sample	Cryogenic time (minutes)	R_b (Ω)	σ (S/cm)
A1	0	0.14	5.7×10^{-2}
A2	2	0.12	6.7×10^{-2}
A3	4	0.10	8.0×10^{-2}

4. Conclusion

This study investigated the effect of cryogenic treatment and rGO incorporation on PVDF–Al_2O_3–CA composite membranes derived from palm kernel shell biomass under aqueous electrochemical screening conditions. Cryogenic treatment significantly refined membrane morphology and reduced bulk resistance. Scanning electron microscopy (SEM) revealed a pore size reduction of approximately 87%, indicating improved structural compactness, while UV–Vis analysis showed an increase in apparent optical band gap from 1.34 eV to 1.44 eV, suggesting enhanced structural ordering within the composite matrix. Electrochemical impedance spectroscopy (EIS) demonstrated a decrease in area-specific bulk resistance from 0.14 to 0.10 Ω·cm^2 after cryogenic treatment, corresponding to an apparent conductivity of 8.0×10^{-2} S cm^{-1} under the applied aqueous configuration. Cyclic voltammetry (CV) results showed that increasing rGO content (Series B) significantly enhanced current response and capacitance behavior, indicating improved interfacial electrochemical activity. These findings suggest that cryogenic processing primarily governs pore refinement and bulk resistance reduction, while rGO incorporation influences interfacial electrochemical response within the composite membrane system. The reported electrochemical parameters represent screening-level behavior under aqueous conditions and do not imply intrinsic lithium-ion electrolyte performance. Further investigation using solid-state lithium configurations is required to evaluate true ionic conductivity and Li^+ transport properties.

Acknowledgement

This research is supported by the Directorate General of Higher Education, Ministry of Education, Culture, Research, and Technology of the Republic of Indonesia through the 2025 Student Creativity Program (PKM) [grant number 1995/B2/DT.01.00/2025, July 3, 2025].

References

[1] J. Suresh, R. V. V. Krishna, V. Satyanarayana, P. S. Ranjit, Advancements in Battery Technology: Quantum Computing Perspectives, in: C. Ananth, T.A. Kumar, O. Ibrahim Khalaf (Eds.) *Real-World Challenges in Quantum Electronics and Machine Computing*, IGI Global Scientific Publishing, Hershey, PA, USA, 2024, https://doi.org/10.4018/979-8-3693-4001-1.ch002

[2] Anji Reddy Polu, Kwangmin Kim, Aseel A. Kareem, Dongkyu Kim, Shufeng Song, Serguei V. Savilov, Pramod K. Singh, Impact of tetracyanoethylene plasticizer on PEO based solid polymer electrolytes for improved ionic conductivity and solid-state lithium-ion battery performance, *Journal of Power Sources*, 625, (2025), 235742 https://doi.org/10.1016/j.jpowsour.2024.235742

[3] Lingfei Tang, Bowen Chen, Zhonghan Zhang, Changqi Ma, Junchao Chen, Yage Huang, Fengrui Zhang, Qingyu Dong, Guoyong Xue, Daiqian Chen, Chenji Hu, Shuzhou Li, Zheng Liu, Yanbin Shen, Qi Chen, Liwei Chen, Polyfluorinated crosslinker-based solid polymer electrolytes for long-cycling 4.5 V lithium metal batteries, *Nature Communications*, 14, 1, (2023), 2301 https://doi.org/10.1038/s41467-023-37997-6

[4] Yanping Li, Tao Yang, Hongxun Wang, Guosheng Wen, Cheng Zhang, Zhicheng Han, Gongjia Lan, Dazhou Yan, Songxuan Chen, Improved Performance of Organic–Inorganic Hybrid Gel Polymer Electrolyte by In Situ Incorporation Based on Poly(vinylidene fluoride-co-hexafluoropropylene) (PVDF-HFP) for Lithium-Ion Batteries, *ACS Omega*, 10, 21, (2025), 21162-21172 https://doi.org/10.1021/acsomega.4c10111

[5] Charlie A. F. Nason, Ajay Piriya Vijaya Kumar Saroja, Yi Lu, Runzhe Wei, Yupei Han, Yang Xu, Layered Potassium Titanium Niobate/Reduced Graphene Oxide Nanocomposite as a Potassium-Ion Battery Anode, *Nano-Micro Letters*, 16, 1, (2023), 1 https://doi.org/10.1007/s40820-023-01222-2

[6] Khizar Hayat Khan, Abdul Haleem, Sajal Arwish, Afzal Shah, Hazrat Hussain, PVDF-based solid polymer electrolytes for lithium-ion batteries: strategies in composites, blends, dielectric engineering, and machine learning approaches, *RSC Advances*, 15, 26, (2025), 20629-20656 https://doi.org/10.1039/d5ra02951a

[7] Jiaqi Lu, Kaihang Zhang, Dinku Hazarika, Liangquan Xu, Jie Li, Jianhui Wu, Muhammad Naeem Shah, Hao Jin, Shurong Dong, Yuhui Huang, Qilong Zhang, Yongjun Wu, Jikui Luo, Synthesis of High-Performance Polyvinylidene Fluoride Composites via Hydroxyl Anchoring Effect and Directional Freeze-Drying Method, *Advanced Energy and Sustainability Research*, 5, 6, (2024), 2300237 https://doi.org/10.1002/aesr.202300237

[8] Shuang Xiang, Lin Zhu, Liang Fu, Miaomiao Wang, Xianbi Zhang, Yougen Tang, Dan Sun, Haiyan Wang, Cryogenic and in situ characterization techniques for electrode interphase analysis, *eScience*, 5, 1, (2025), 100291 https://doi.org/10.1016/j.esci.2024.100291

[9] Ahmed M. El-Khawaga, Hesham Tantawy, Mohamed A. Elsayed, Ahmed I. A. Abd El-Mageed, Synthesis and applicability of reduced graphene oxide/porphyrin nanocomposite as photocatalyst for waste water treatment and medical applications, *Scientific Reports*, 12, 1, (2022), 17075 https://doi.org/10.1038/s41598-022-21360-8

[10] Ersu Lökçü, Süleyman Can, Mustafa Anik, Ultrasound-assisted synthesis of rGO/SiO_2-based nanosheets and their electrochemical performances in Li-ion batteries, *Turkish Journal of Chemistry*, 47, 2, (2023), 495-503 https://doi.org/10.55730/1300-0527.3554

[11] Tao Chen, Yuncong Liu, Zhekai Jin, Lin Sun, Zeyu Liu, Hao Xu, Zhiguo Zhao, Chao Wang, Solid polymer electrolytes regulated by ion-dipole interactions for high voltage lithium batteries, *Giant*, 19, (2024), 100310 https://doi.org/10.1016/j.giant.2024.100310

[12] Assem Mubarak, Bayandy Sarsembayev, Yerzhigit Serik, Abdirakhman Onabek, Zhanat Kappassov, Zhumabay Bakenov, Kazuyoshi Tsuchiya, Gulnur Kalimuldina, Quenched PVDF/PMMA Porous Matrix for Triboelectric Energy Harvesting and Sensing, *Energy & Environmental Materials*, 8, 1, (2025), e12808 https://doi.org/10.1002/eem2.12808

[13] Jiewen Tan, Xin Ao, Hao Zhuo, Libin Zhuang, Xiao Huang, Chenliang Su, Wei Tang, Xinwen Peng, Bingbing Tian, Cryogenic engineering of solid polymer electrolytes for room temperature and 4 V-class all-solid-state lithium batteries, *Chemical Engineering Journal*, 420, (2021), 127623 https://doi.org/10.1016/j.cej.2020.127623

[14] Zahid Mehmood, Syed Aizaz Ali Shah, Saeed Omer, Ramsha Idrees, Shaukat Saeed, Scalable synthesis of high-quality, reduced graphene oxide with a large C/O ratio and its dispersion in a chemically modified polyimide matrix for electromagnetic interference shielding applications, *RSC Advances*, 14, 11, (2024), 7641-7654 https://doi.org/10.1039/d4ra00329b

[15] Syahrul Humaidi, Syarah Aldira, Titik Lestariningsih, Manufacture of Solid Polymer Electrolyte (SPE) Based on PVDF HFP-LiBOB, *Journal of Technomaterial Physics*, 4, 2, (2022), 117-121 https://doi.org/10.32734/jotp.v4i2.8250

[16] Anseong Park, Je-Yeon Jung, Seungtae Kim, WooJin Kim, Min Young Seo, Sangdeok Kim, YongJoo Kim, Won Bo Lee, Crystallization behavior of polyvinylidene fluoride (PVDF) in NMP/DMF solvents: a molecular dynamics study, *RSC Advances*, 13, 19, (2023), 12917-12924 https://doi.org/10.1039/D3RA00549F

[17] Aldo Kevin López-Matus, Viridiana Wendy Velázquez Vázquez, Karla María Aguilar-Casto, Edgar Vicente Macias-Melo, Getsemani Morales Mendoza, José Ysmael Verde Gómez, Rosendo López-González, Enhanced photocatalytic activity of rGO-WO_3 for hydrogen generation through copper oxide incorporation under sunlight irradiation, *Journal of Materials Science: Materials in Engineering*, 20, 1, (2025), 75 https://doi.org/10.1186/s40712-025-00290-z

[18] Christofer Sångeland, Guiomar Hernández, Daniel Brandell, Reza Younesi, Maria Hahlin, Jonas Mindemark, Dissecting the Solid Polymer Electrolyte–Electrode Interface in the Vicinity of Electrochemical Stability Limits, *ACS Applied Materials & Interfaces*, 14, 25, (2022), 28716-28728 https://doi.org/10.1021/acsami.2c02118

[19] Lei Zhang, Yao Dai, Chao Li, Yuzhen Dang, Runguo Zheng, Zhiyuan Wang, Yuan Wang, Yanhua Cui, Hamidreza Arandiyan, Zongping Shao, Hongyu Sun, Quanchao Zhuang, Yanguo Liu, Recent advances in electrochemical impedance spectroscopy for solid-state batteries, *Energy Storage Materials*, 69, (2024), 103378 https://doi.org/10.1016/j.ensm.2024.103378

[20] Naveed Ahmed, Muhammad Huzaifa Raza, Muhammad Asad Ali, Waseem Tahir, Ateekh Ur Rehman, Analyzing the dimensional errors in wire electric discharge machining of squeeze casted

Al2024/Al_2O_3/W composite using cryogenic treated electrodes, *Journal of Materials Research and Technology*, 29, (2024), 476-490 https://doi.org/10.1016/j.jmrt.2024.01.125

[21] Rafi Athallah, Sylvia Ayu Pradanawati, Reffy Aldo Amanta, Azzah Dyah Pramata, Nezihe Ayas, Tetsuya Kida, Nur Laila Hamidah, The Role of Graphene Oxide as a Filler and Lanthanum Nitrate as a Salt in Corn Starch-Based Solid Polymer Electrolytes, *International Journal of Technology*, 16, 2, (2025), 291-319 https://doi.org/10.14716/ijtech.v16i2.7294

[22] Sergey Fomin, Evgenia Shirokova, Iren Kraeva, Ivan Tolstobrov, Andrey Bushuev, Kirill Yuzhanin, Boris Ananchenko, Alexandre A. Vetcher, Alexey Iordanskii, Effect of Polyvinylidene Fluoride Membrane Production Conditions on Its Structure and Performance Characteristics, *Polymers*, 14, 23, (2022), 5283 https://doi.org/10.3390/polym14235283

[23] Asri Saleh, Fadhil Asy'ari Amhadin, Iin Novianty, Synthesis of Reduced Graphene Oxide and Zinc Oxide Composite From Candlenut Shell Charcoal (*Aleuritas moluccana*), *Elkawnie: Journal of Islamic Science Technology*, 8, 1, (2022), 1-11 https://dx.doi.org/10.22373/ekw.v8i1.9405

[24] Saad Zafar, Sanjana Krishna Mani, Monisha Monisha, Bimlesh Lochab, Concentration-dependent kinetic study of graphene oxide (GO) reduction using biophenol and electrochemical analysis, *RSC Sustainability*, 3, 1, (2025), 365-375 https://doi.org/10.1039/d4su00430b

[25] Suting Weng, Yejing Li, Xuefeng Wang, Cryo-EM for battery materials and interfaces: Workflow, achievements, and perspectives, *iScience*, 24, 12, (2021), https://doi.org/10.1016/j.isci.2021.103402

[26] Chuanyin Xiong, Tianxu Wang, Jing Han, Zhao Zhang, Yonghao Ni, Recent Research Progress of Paper-Based Supercapacitors Based on Cellulose, *Energy & Environmental Materials*, 7, 3, (2024), e12651 https://doi.org/10.1002/eem2.12651

[27] Bich Ngoc Tran, Yasemin Fadil, Yin Yao, Vipul Agarwal, Per B. Zetterlund, Effect of high filler loading on polymer/(reduced) graphene oxide nanocomposite coatings, *RSC Applied Interfaces*, 2, 5, (2025), 1248-1258 https://doi.org/10.1039/d5lf00078e

[28] Alejandro Rivera-Pousa, José Manuel Otero-Mato, Hadrian Montes-Campos, Trinidad Méndez-Morales, Diddo Diddens, Andreas Heuer, Luis Miguel Varela, Ternary Solid Polymer Electrolytes at the Electrochemical Interface: A Computational Study, *Macromolecules*, 57, 9, (2024), 3921-3936 https://doi.org/10.1021/acs.macromol.3c02669